ACS Macro Letters

Letter

pubs.acs.org/macroletters

One-Pot Preparation of Monolithic Molecular Separation Membranes with Sub-10 nm Reticulated Pores Using Concentration-Polarization-Induced Gelation of Covalent Network Nanoparticles

Jae-Sung Bae, Eunkyung Jeon, Minseon Byeon, and Ji-Woong Park*

School of Materials Science and Engineering, Gwangju Institute of Science and Technology, 123 Cheomdan-gwagiro, Buk-gu, Gwangju, 500-712, Korea

Supporting Information

ABSTRACT: Monolithic molecular separation membranes were prepared by utilizing concentration polarization-induced gelation of a particulate covalent network on a porous support. Polymerization of tetra-amine and di-isocyanate monomers produced a stable dispersion of nanoparticles of urea-bonded networks in organic solvent. As the sols were allowed to pass through the support, the critical gelation point was reached due to concentration polarization via accumulation of relatively larger network particles on the substrate surface, resulting in deposition of a nanoporous gel layer, which, upon drying, turned to a monolithic layer of a covalent network with interconnected pores estimated to be 2−10 nm wide. The resulting membrane filters off solutes larger than 3 nm. Facile control of the structure and thickness of the active layer along with the superior chemical and thermal stability are promising features for solvent-resistant nanofiltration membranes suitable for separation of organic, as well as aqueous, solution mixtures.

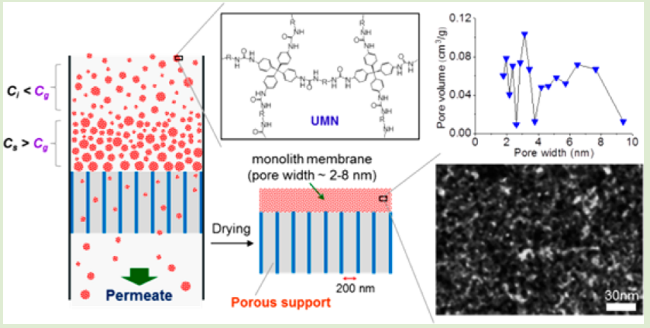

Nanoporous membranes have attracted much attention owing to their wide range of potential applications for molecular separation, energy storage, drug delivery, sensors, and catalysis.[1−6] Among different types of membranes developed to date, the thin-film composite (TFC) membrane format comprised of a thin active barrier layer and a porous support layer has been widely used. The key advantage of the TFC membrane is that both the top selective layer and the bottom porous support can be independently tailored to achieve desired selectivity and permeability along with sufficient mechanical strength.[1,7−11] The active layers of these membranes have been prepared from various types of porous or nonporous materials by interfacial polymerization,[1,11−13] layer-by-layer (LBL) deposition,[14,15] chemical vapor deposition,[16,17] or growth of thin film crystals.[18−20] They were demonstrated for selective separation of small molecular species in desalination, pervaporation, or gas separation.

Nanoporous separation layers have often been fabricated using conventional phase-separation-based methods; however, it is usually difficult to obtain the active layer with a pore width smaller than 10 nm.[21−23] In simple homopolymer blends in solutions or melts, it is difficult to arrest coarsening of the phase-separated microdomains to a macroscopic level due to high molecular mobility in these soft material states. A multitude of other approaches using block copolymer,[24,25] liquid crystals,[21] carbon nanotubes,[22,26] nanoparticles,[23] and other materials[27,28] have been developed to form a mesoporous separation layer on top of the support with larger pores. Nevertheless, these methods usually lack scalability, and therefore, a simpler approach to the formation of a porous layer in sub-10 nm scale is still demanded.

It is highly important that the sub-10 nm porous organic structure must possess dimensional stability against heat or chemicals.[11,29,30] Polymer−solvent interfaces are not atomically sharp as the metallic or ceramic surface in an organic solvent because organic solvent−polymer interaction parameters are generally in the range allowing the solvent to penetrate the polymer surface to the depth of several nanometers that is smaller than the typical length (5−10 nm) between entanglements of flexible polymer chains. This means that sub-10 nm polymeric structures can be easily deformed or damaged by organic solvent. The small nanostructure with high surface area is even more unstable at elevated temperatures. Chemical cross-linking of the polymeric membrane usually enhances the thermal or chemical resistance,[11,30−33] but the pores on the nanometer scale can still be deformed by exposure to heat or chemicals unless the cross-linking is sufficiently dense on the molecular level. A variety of known molecular-level organic or inorganic networks with sub-10 nm pore structures, such as zeolites, covalent organic frameworks (COFs), and porous polymer networks (PPNs),[19,34−38] are obtained usually

Received: June 30, 2015
Accepted: August 25, 2015
Published: August 27, 2015

DOI: 10.1021/acsmacrolett.5b00430
ACS Macro Lett. 2015, 4, 991−995

as intractable solids and it is thus difficult to process them into defect-free, thin-film membranes on a sufficiently large area.

New approaches to a solution-processable covalent molecular network have been developed in recent years to obtain freestanding films or particles.[39−42] In particular, in the organic sol−gel (OSG) method developed recently,[39−41] network-forming monomers are polymerized in organic solvent to produce dispersions (sols) of nanoparticulate networks. Below a critical gelation concentration (c_g), the molecular scale networks grow dendritically to form stable nanoparticles. The reactive functional groups on the surface of the nanoparticles bond together, leading to a monolith of covalent molecular networks in thin film as the sol was cast on the substrate and subsequently dried. Unfortunately, the free-standing films obtained by drop-casting of the sols were hardly permeable to liquids and gases,[40] due to the formation of a dense network matrix. Constructing nanometer-scale through-channels across the covalently networked matrices is essential for exploitation of the potential of the new solution-processable network materials.

Here we present a one-pot method for preparing a nanoporous film from the sol of growing covalent network. We utilize that the covalent networks comprising the nanoparticles formed by polymerization of multifunctional monomers are dendritic and incompletely cross-linked. As the network nanoparticles are passed through a porous polymer support, smaller particles of premature networks are removed by permeation, while larger particles are concentrated on top of the surface to yield a gel layer. The resulting composite membranes contain three-dimensionally reticulated pores in a width of several nanometers. The nanoporous structure of the membranes was resistant to organic solvent and exhibited efficient rejection of solutes larger than 3 nm. The thermal and chemical resistance of the nanopore structure with facile pore size tunability and scalability is promising for advanced membrane-based technologies.

To obtain a sol of growing covalent network, we polymerized equivalent amounts of tetrakis(4-aminophenyl)methane (TAPM) and hexamethylene diisocyanate (HDI) in DMF (Figure 1a).[39,40] The monomer mixture was stirred shorter than the gelation time (t_g), that is, the time that it takes for the initial monomer solution to become a gel, to yield nanoparticle dispersions of urea-based molecular networks (UMNs). For example, the current UMN sol employed for membrane fabrication was prepared by stirring the monomer solution for 75 h, which was less than the t_g (85 h) for a TAPM/HDI mixture of 0.04 g/mL in DMF. The solution was then diluted with DMF to a concentration (0.01 g/mL) below the critical gelation concentration (c_g, 0.03 g/mL for TAPM/HDI in DMF), by which the networks would essentially stop growing further and maintain the fluid sol state. The average size of the UMN particles in the sol was about 90 nm, as determined by dynamic light scattering (DLS). We used the diluted sol for preparation of the membranes, as described below.

The UMN nanoparticles in the sol state contain reactive termini on their surface; hence, the interparticle network will grow via condensation reactions when a chemical or physical stimulus makes the particles become aggregated.[43−45] In the present study, we utilized the phenomenon of concentration polarization to drive the interparticle networking reaction. Concentration polarization is the phenomenon that the concentration of solutes at the feed side surface of a transport membrane increases as the transport of the solute is hindered

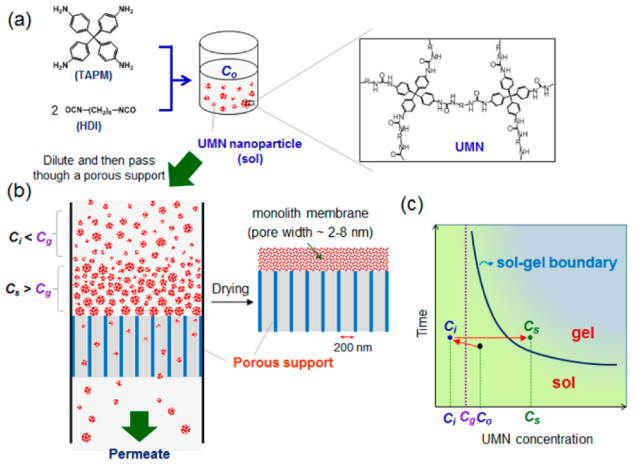

Figure 1. Spontaneous deposition of the nanoporous network layer by concentration-polarization-induced gelation of a living covalent network sol. (a) Cross-linking polymerization of TAPM and HDI below a critical gelation point to obtain nanoparticulate dispersion (sol) of a urea-bonded molecular network (UMN). (b) UMN sol was diluted and then passed through a porous nylon support with an average pore size of 200 nm. The resultant UMN gel/nylon composite film was removed from the filter and dried to yield a thin film composite membrane with a UMN active layer. (c) Time−concentration diagram for the sol-to-gel transformation, where c_g, c_o, c_i, and c_s are the critical gelation concentration, the concentration of original polymerizing solution, the initial dilute concentration, and the concentration on the support surface, respectively, of the UMN nanoparticles. The curve is the sol−gel boundary obtained by connecting the gelation times (t_g) measured at various concentrations of the network.

by the membranes.[46,47] We anticipated that as the sol of UMN nanoparticles passes through such a substrate having pores larger than the particles but small enough to delay their transport, the nanoparticles would become concentrated on the feed-side surface of the support. Because the transport hindrance is greater to the larger UMN particles, the particles are concentrated on the porous support while being sorted by their size, as shown schematically in Figure 1b. Smaller particles of premature networks are removed by permeation. Hindered transport of particles increases the concentration on the support surface from c_i to c_s in Figure 1c, making the critical gelation point (c_g) to be crossed; hence, the sols concentrated on the support surface become gelled spontaneously (Figure 1c). Subsequent drying of the gel-coated polymer membrane will resume covalent condensation between the network particles to form a thin monolithic coating on the porous support, of which the spaces within dendritic particulate networks are interconnected macroscopically while yielding three-dimensionally reticulated nanopores.

The diluted UMN sol was permeated through a nylon membrane (average pore size, 200 nm) by compressing it with nitrogen gas at 0.5 bar (Figure 1b). The flux decreased with the permeation volume of the sol (Figure 2a). The solid content in each of the permeated solution fractions decreased with increasing the permeation time, indicating that the deposition rate of the UMNs over the support increased as the sol continued to be passed through. Dynamic light scattering (DLS) curves for the solution fractions collected after permeation of the sol indicate that the concentration polarization on the porous surface of the support made the particles sort in the order of their diameter (Figure 2b). For

DOI: 10.1021/acsmacrolett.5b00430
ACS Macro Lett. 2015, 4, 991−995

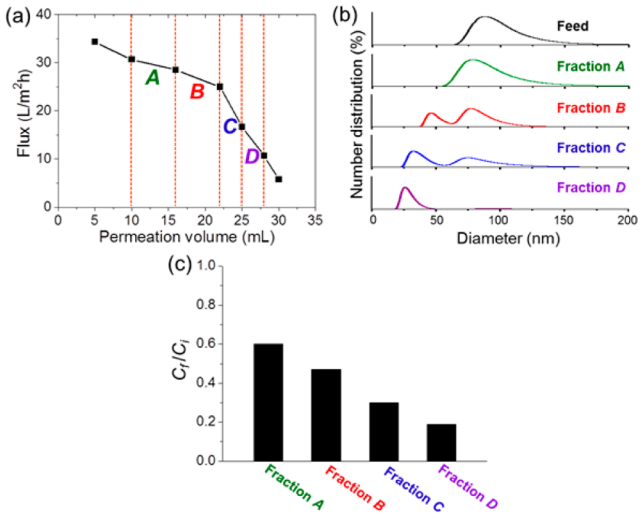

Figure 2. Flux of urea molecular network (UMN) sols permeated through a porous nylon-6,6 support and the distribution in the size of residual UMN particles in permeated solutions. (a) Permeate flux of UMN sol through the nylon membrane was observed to decrease with increasing permeation volume during the deposition. (b) Size distribution of the residual particles determined by DLS was observed to shift to the smaller diameter for the later fractions, indicating that smaller particles were becoming more difficult to pass the membrane at longer permeation times. (c) Ratio of the concentration (C_f) of each permeated fraction to the initial solution concentration (C_i). The solid content was estimated by evaporation and drying of the permeated solution.

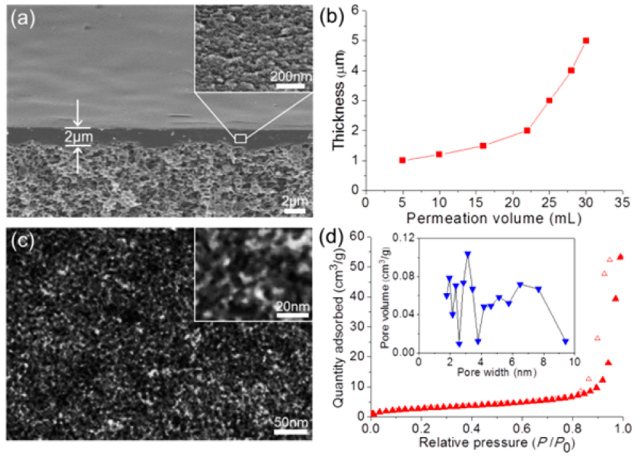

Figure 3. Structure of nanoporous monolith membranes. (a) Cross-sectional SEM (at 40° tilt) image of the nanoporous composite membrane with a UMN layer thickness of 2 μm. Inset shows a magnified SEM image of the UMN layer. (b) Thickness of the UMN layer deposited by varying the volume of the UMN sol permeated through the membrane. (c) Cross-sectional TEM image of the composite membrane. An ultrathin section was obtained by microtoming and stained with ruthenium tetroxide (RuO_4). Inset shows a magnified TEM image. (d) N_2 adsorption−desorption isotherms of the UMN layer (after nylon support was stripped with *m*-cresol) measured at 77 K. Inset shows pore size distribution with $dV/d\log(w)$ pore volume on the *y*-axis. The BET surface area and pore volume of the UMN top layer were 27.5 m^2/g and 0.1 cm^3/g, respectively. The pore volume was calculated by the BJH method from the desorption branch of the nitrogen isotherm.

example, the solid content in the latest permeated fraction was about 20% of that in the stock solution (Figure 2c), and the peak diameter of the UMN particle in the same fraction was about 25 nm, which was much smaller than the original value (90 nm) of the stock solution (Figure 2b). This means that the support surface is deposited with larger UMN particles, while the smaller particles, most likely oligomeric networks, are removed from the deposited layer.

After deposition of an appropriate thickness of the gel layer, the samples were removed from the filtration kit and dried by stepwise heating (see the Experimental Section in the Supporting Information). Scanning electron microscopy (SEM) images of the dried UMN layer indicate the formation of a compact solid film (Figure 3a) over the porous nylon support. The thickness of the network layer (Figure S1, Supporting Information) could be adjusted by varying the total volume of the UMN sol passed through the support membrane (Figure 3b). To obtain a defectless large area membrane from the 0.01 g/mL UMN sol, a layer with a thickness of at least 2 μm had to be deposited. An atomic force microscope (AFM) image of the top surface showed low roughness with no pinholes or cracks (Figure S3). A transmission electron microscopy (TEM) image (Figure 3c and Figure S2, Supporting Information) of an ultrathin cross-section of the UMN layer shows that the three-dimensionally interconnected pores of approximately several nanometers wide are present throughout the matrix. The porosity of the membrane was further analyzed after stripping the nylon support from the composite membrane with *m*-cresol (Figure S4, Supporting Information, for confirmation of the removal of the nylon support by *m*-cresol treatment). The pore size of the resulting UMN layer was in the range of 2−10 nm, as estimated by the Barrett−Joyner−Halenda (BJH) method (Figure 3d and Figure S5, Supporting Information),[48,49] being consistent with the TEM image.

The UMN particles are soft microgels containing nanoscale space filled with solvent. The height of the dry UMN nanoparticles appeared to be much smaller than their diameter as shown by the atomic force microscope (AFM) images of the particles captured on a silicon wafer from their sol state (Figure S6, Supporting Information). Upon drying, they are collapsed by expulsion of solvent from the interior of the particles. This suggests that the nanopores are originated from an unfilled space within the UMN nanoparticles. Initial dendritic particulate networks are interconnected three-dimensionally while generating monoliths with reticulated nanopores throughout.

The size of the UMN particles in the initial sol mixture appeared to be critical for successful preparation of the nanoporous membranes. For instance, a UMN sol prepared by reacting the monomer shorter than 50 h resulted in incomplete coverage of the porous support, most likely due to the size of UMN nanoparticles in the premature sols[39−41] that is too small to induce concentration polarization on the porous support. The sols of smaller UMN particles should need different optimization of conditions, such as flux, initial concentration, and permeation volume, for preparation of the composite membrane with desired structure.

The present UMN membrane is distinct from the polymeric gel layer in a recent report,[50] where a molecular separation membrane of a cross-linked cationic polymer gel has been deposited on a porous sacrificial layer and then the sacrificial layer is removed by dissolving it with solvent. Our membranes form via spontaneous gelation of the covalent network on the support surface with no use of a sacrificial layer or cross-linking

DOI: 10.1021/acsmacrolett.5b00430
ACS Macro Lett. 2015, 4, 991−995

agents. The resulting membrane is also very different from the cross-linked polymer membrane in their molecular level structure. The three-dimensionally interconnected nanopores form across the monolithic film of the molecularly cross-linked network, and hence, they possess superior dimensional stability in both organic and aqueous solvents, even at elevated temperatures, as discussed below.

To evaluate the separation performance of each of the UMN composite membranes, solutes with known size, such as glucose, mono-6-*O*-(*p*-toluenesulfonyl)-γ-cyclodextrin (Ts-γ-CD), cytochrome c (Cyt), bovine serum albumin (BSA), and silica nanoparticles (Figure 4a), were filtered through the

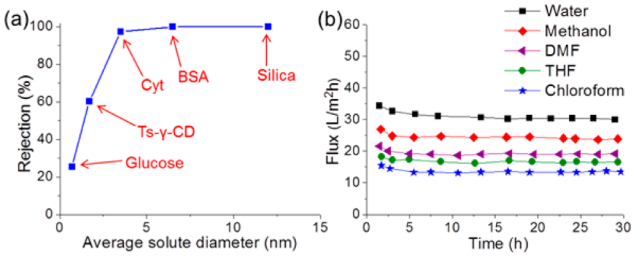

Figure 4. Filtration of solute and permeation of various solvents through UMN composite membranes. (a) Rejection of different solutes dissolved in aqueous solutions by the composite membrane at 5 bar. The solute rejection (i.e., the percentage (%) of the solute that the membrane prevented from passing through) was plotted as a function of average solute diameter. (b) Permeation of organic solvents and water through the composite membrane at 5 bar.

membranes. A detailed description of this performance test is given in Experimental Section in the Supporting Information. The composite membranes nearly completely prevented solutes greater than 3 nm in diameter from passing through. While Cyt, BSA, and the larger silica particles were filtered off by the composite membrane with a UMN layer thicker than 2 μm, glucose and Ts-γ-CD passed through the membrane. Supporting Information, Table S1, summarizes the separation performance of the composite membranes. The composite membrane was observed to be highly permeable to organic liquids as well as water (Figure 4b). The films deposited thicker than 4 μm were impermeable to liquid even at high operating pressures (Table S1, Supporting Information). We postulate that oligomeric nanoparticles of premature networks fill up the pores in thick membranes. Steady-state flux of various organic solvents through the membrane persisted for long periods of time, indicative of the resistance of the membrane to being degraded by these solvents. The flux of a liquid through the membrane varied slightly with the molecular weight and polarity of the solvent. The thermal degradation temperature of the dry membranes appeared to be greater than 300 °C, according to thermogravimetric analysis (TGA; Figure S7, Supporting Information). The membrane treated in 200 °C NMP for 30 h showed no deterioration of permeation property. The water flux measured after the treatment was nearly the same as that before the treatment (Figure S8, Supporting Information), indicative of the chemical and thermal resistance of the nanoporous structure in the monolith membrane.

In principle, the UMN sols can be prepared from different pairs of amine and isocyanate monomers at various concentrations. In addition, the average size of particles in the sols varies with the aging (reaction) time of the sols.[39−41] These variables can be used to control the thickness and the porosity of the UMN active layer. The variety of porous organic or inorganic supports that are currently available will further improve the tunability of our membrane fabrication method. Future study will need to focus on reducing the thickness of the network layer with increasing the porosity for enhancement of the flux of the membrane to a practically useful level.

In summary, we have presented a facile method for producing a nanoporous composite membrane using concentration polarization to induce gelation of organic sols of covalent molecular networks on a porous support. The thickness of the active layer and the porosity of the network membrane can be easily controlled by adjusting the volume of the network sols used for the formation of the active layer. The membranes that we produced by the one-pot method possess pores in the sub-10 nm range. The superior chemical and thermal stability of these membranes and, hence, of their nanoporosity, conferred by the covalent networks, is a promising feature for wider application of the membrane in the separation of both organic and aqueous mixtures.

■ ASSOCIATED CONTENT

Supporting Information

The Supporting Information is available free of charge on the ACS Publications website at DOI: 10.1021/acsmacrolett.5b00430.

Experimental details, SEM, TEM, and AFM images of composite membrane, membrane performance, and flux results after solvent and heat treatment (PDF)

■ AUTHOR INFORMATION

Corresponding Author

*E-mail: jiwoong@gist.ac.kr.

Notes

The authors declare no competing financial interest.

■ ACKNOWLEDGMENTS

This research was supported by the Basic Science Research Program (2010-0026421) and the Global Frontier Program through Global Frontier Hybrid Interface Materials (2013M3A6B1078869) of the National Research Foundation of Korea (NRF) funded by the Ministry of Science, ICT & Future Planning.

■ REFERENCES

(1) Marchetti, P.; Jimenez Solomon, M. F.; Szekely, G.; Livingston, A. G. *Chem. Rev.* **2014**, *114*, 10735−10806.
(2) Lee, H.; Yanilmaz, M.; Toprakci, O.; Fu, K.; Zhang, X. *Energy Environ. Sci.* **2014**, *7*, 3857−3886.
(3) Lo, K.-H.; Chen, M.-C.; Ho, R.-M.; Sung, H.-W. *ACS Nano* **2009**, *3*, 2660−2666.
(4) Kirsch, J.; Siltanen, C.; Zhou, Q.; Revzin, A.; Simonian, A. *Chem. Soc. Rev.* **2013**, *42*, 8733−8768.
(5) Cantone, S.; Ferrario, V.; Corici, L.; Ebert, C.; Fattor, D.; Spizzo, P.; Gardossi, L. *Chem. Soc. Rev.* **2013**, *42*, 6262−6276.
(6) Vankelecom, I. F. J. *Chem. Rev.* **2002**, *102*, 3779−3810.
(7) Krogman, K. C.; Lowery, J. L.; Zacharia, N. S.; Rutledge, G. C.; Hammond, P. T. *Nat. Mater.* **2009**, *8*, 512−518.
(8) Fane, A. G.; Wang, R.; Hu, M. X. *Angew. Chem., Int. Ed.* **2015**, *54*, 3368−3386.
(9) Gu, J.-E.; Lee, S.; Stafford, C. M.; Lee, J. S.; Choi, W.; Kim, B.-Y.; Baek, K.-Y.; Chan, E. P.; Chung, J. Y.; Bang, J.; Lee, J.-H. *Adv. Mater.* **2013**, *25*, 4778−4782.

DOI: 10.1021/acsmacrolett.5b00430
ACS Macro Lett. 2015, 4, 991−995

(10) Nagale, M.; Kim, B. Y.; Bruening, M. L. *J. Am. Chem. Soc.* **2000**, *122*, 11670−11678.
(11) Vandezande, P.; Gevers, L. E. M.; Vankelecom, I. F. J. *Chem. Soc. Rev.* **2008**, *37*, 365−405.
(12) Zhou, C.; Shi, Y.; Sun, C.; Yu, S.; Liu, M.; Gao, C. *J. Membr. Sci.* **2014**, *471*, 381−391.
(13) Lee, K. P.; Arnot, T. C.; Mattia, D. *J. Membr. Sci.* **2011**, *370*, 1−22.
(14) Joseph, N.; Ahmadiannamini, P.; Hoogenboom, R.; Vankelecom, I. F. J. *Polym. Chem.* **2014**, *5*, 1817−1831.
(15) Tamaddondar, M.; Pahlavanzadeh, H.; Saeid Hosseini, S.; Ruan, G.; Tan, N. R. *J. Membr. Sci.* **2014**, *472*, 91−101.
(16) Kase, T.; Ogino, T. *J. Phys. Chem. C* **2013**, *117*, 15991−15995.
(17) Lin, X.; Liu, P.; Wei, Y.; Li, Q.; Wang, J.; Wu, Y.; Feng, C.; Zhang, L.; Fan, S.; Jiang, K. *Nat. Commun.* **2013**, *4*, n/a DOI: 10.1038/ncomms3920.
(18) Sato, K. *J. Membr. Sci.* **2008**, *307*, 181.
(19) Huang, A.; Dou, W.; Caro, J. *J. Am. Chem. Soc.* **2010**, *132*, 15562−15564.
(20) Bradshaw, D.; Garai, A.; Huo, J. *Chem. Soc. Rev.* **2012**, *41*, 2344−2381.
(21) Zhou, M.; Kidd, T. J.; Noble, R. D.; Gin, D. L. *Adv. Mater.* **2005**, *17*, 1850−1853.
(22) Hinds, B. J.; Chopra, N.; Rantell, T.; Andrews, R.; Gavalas, V.; Bachas, L. G. *Science* **2004**, *303*, 62−65.
(23) Zhang, Q.; Ghosh, S.; Samitsu, S.; Peng, X.; Ichinose, I. *J. Mater. Chem.* **2011**, *21*, 1684−1688.
(24) Jackson, E. A.; Hillmyer, M. A. *ACS Nano* **2010**, *4*, 3548−3553.
(25) Jackson, E. A.; Lee, Y.; Hillmyer, M. A. *Macromolecules* **2013**, *46*, 1484−1491.
(26) Zhang, X. *Adv. Mater.* **2008**, *20*, 4140−4144.
(27) Krieg, E.; Weissman, H.; Shirman, E.; Shimoni, E.; Rybtchinski, B. *Nat. Nanotechnol.* **2011**, *6*, 141−146.
(28) Karan, S.; Samitsu, S.; Peng, X.; Kurashima, K.; Ichinose, I. *Science* **2012**, *335*, 444−447.
(29) Darvishmanesh, S.; Firoozpour, L.; Vanneste, J.; Luis, P.; Degreve, J.; Bruggen, B. V. d. *Green Chem.* **2011**, *13*, 3476−3483.
(30) Szekely, G.; Jimenez-Solomon, M. F.; Marchetti, P.; Kim, J. F.; Livingston, A. G. *Green Chem.* **2014**, *16*, 4440−4473.
(31) Wu, D.; Xu, F.; Sun, B.; Fu, R.; He, H.; Matyjaszewski, K. *Chem. Rev.* **2012**, *112*, 3959−4015.
(32) Vanherck, K.; Vandezande, P.; Aldea, S. O.; Vankelecom, I. F. J. *J. Membr. Sci.* **2008**, *320*, 468−476.
(33) Yang, S. Y.; Park, J.; Yoon, J.; Ree, M.; Jang, S. K.; Kim, J. K. *Adv. Funct. Mater.* **2008**, *18*, 1371−1377.
(34) Yao, J.; Wang, H. *Chem. Soc. Rev.* **2014**, *43*, 4470−4493.
(35) Ding, S.-Y.; Wang, W. *Chem. Soc. Rev.* **2013**, *42*, 548−568.
(36) Lu, W.; Yuan, D.; Sculley, J.; Zhao, D.; Krishna, R.; Zhou, H.-C. *J. Am. Chem. Soc.* **2011**, *133*, 18126−18129.
(37) Ben, T.; Ren, H.; Ma, S.; Cao, D.; Lan, J.; Jing, X.; Wang, W.; Xu, J.; Deng, F.; Simmons, J. M.; Qiu, S.; Zhu, G. *Angew. Chem., Int. Ed.* **2009**, *48*, 9457−9460.
(38) Colson, J. W.; Woll, A. R.; Mukherjee, A.; Levendorf, M. P.; Spitler, E. L.; Shields, V. B.; Spencer, M. G.; Park, J.; Dichtel, W. R. *Science* **2011**, *332*, 228−231.
(39) Moon, S.-Y.; Bae, J.-S.; Jeon, E.; Park, J.-W. *Angew. Chem., Int. Ed.* **2010**, *49*, 9504−9508.
(40) Moon, S.-Y.; Jeon, E.; Bae, J.-S.; Byeon, M.; Park, J.-W. *Polym. Chem.* **2014**, *5*, 1124−1131.
(41) Moon, S.-Y.; Mo, H.-R.; Ahn, M.-K.; Bae, J.-S.; Jeon, E.; Park, J.-W. *J. Polym. Sci., Part A: Polym. Chem.* **2013**, *51*, 1758−1766.
(42) Zheng, J.; He, Q.; Liu, C.; Yuan, T.; Zhang, S.; Yang, H. *J. Membr. Sci.* **2015**, *476*, 571−579.
(43) Lin, M. Y.; Lindsay, H. M.; Weitz, D. A.; Ball, R. C.; Klein, R.; Meakin, P. *Nature* **1989**, *339*, 360−362.
(44) Lu, P. J.; Zaccarelli, E.; Ciulla, F.; Schofield, A. B.; Sciortino, F.; Weitz, D. A. *Nature* **2008**, *453*, 499−503.
(45) Li, L.; Miesch, C.; Sudeep, P. K.; Balazs, A. C.; Emrick, T.; Russell, T. P.; Hayward, R. C. *Nano Lett.* **2011**, *11*, 1997−2003.
(46) Beck, R. E.; Schultz, J. S. *Science* **1970**, *170*, 1302−1305.
(47) Davidson, M. G.; Deen, W. M. *Macromolecules* **1988**, *21*, 3474−3481.
(48) Barrett, E. P.; Joyner, L. G.; Halenda, P. P. *J. Am. Chem. Soc.* **1951**, *73*, 373−380.
(49) Huang, B.; Bartholomew, C. H.; Woodfield, B. F. *Microporous Mesoporous Mater.* **2014**, *184*, 112−121.
(50) Wang, Q.; Samitsu, S.; Ichinose, I. *Adv. Mater.* **2011**, *23*, 2004−2008.

DOI: 10.1021/acsmacrolett.5b00430
ACS Macro Lett. 2015, 4, 991−995